Effects of local stress fields around broken fibres on the longitudinal failure of composite materials

Rodrigo P. Tavares[a,b,c], Jose M. Guerrero[b], Fermin Otero[c,d], Albert Turon[b], Joan A. Mayugo[b], Josep Costa[b], Pedro P. Camanho[a,c]

[a] *DEMec, Faculdade de Engenharia, Universidade do Porto, Rua Dr. Roberto Frias, 4200-465 Porto, Portugal*
[b] *AMADE, Polytechnic School, University of Girona, Campus Montilivi s/n, 17071 Girona, Spain*
[c] *INEGI, Rua Dr. Roberto Frias, 400, 4200-465 Porto, Portugal*
[d] *Centre Internacional de Mètodes Numèrics a l'Enginyeria (CIMNE), Edifici C1, Campus Nord UPC C/ Gran Capità S/N, 08034 Barcelona, Spain*

Abstract

An in-depth analysis of the stress fields that surround a broken fibre in fibre reinforced composites is performed and the effects of different material properties are analysed. The stress fields obtained using a spring element model with a random distribution are compared with analytical formulations present in the literature, within a progressive failure model framework. This analysis is then extended to clusters of broken fibres with different sizes and the evolution of the stress fields are analysed. Finally, material macro behaviour and cluster formation is analysed using the spring element model and the progressive failure model framework. The authors found that while for the spring element model the stress redistribution and material behaviour changes with the main material parameters, the same was not found to be true using the analytical formulations for stress concentration and ineffective length. Furthermore, it was found that the current definition for a cluster of broken fibres can lead to erroneous results, depending on the material system.

Keywords: Micro-mechanics, Modelling, Composite materials

*Corresponding author
Email address: pcamanho@fe.up.pt (Pedro P. Camanho)

1. Introduction

As the main load carrying component, fibres play a fundamental role in failure of composite materials. It is widely accepted that fibre strength is a stochastic property [1, 3**?**] and that longitudinal tensile failure of composite materials is dominated by the formation of clusters of broken fibres [4–8]. The formation of clusters of broken fibres depends not only on the fibre strength statistics but also on the stress redistribution after a fibre breaks [9]. A broken fibre only looses its load carrying capability within a small region, denominated ineffective length [10, 11]. Within this region the surrounding intact fibres need to support the loss of load carrying capability of the broken fibre and are, therefore, subjected to stress concentration. This stress redistribution depends on the matrix's ability to transfer stress to the intact fibres and back to the broken fibre itself by shear. The redistribution of stress is the main factor affecting the creation of clusters of broken fibres, which makes it necessary to have accurate models for stress redistribution to correctly capture the failure phenomena.

There are several different models available in the literature. Depending on how the stress from a broken fibre is redistributed the models can be considered global load sharing models (GLS) [12–14], if the stress of the broken fibre is equally distributed to all intact fibres, or local load sharing models (LLS) [6, 10, 15–24] if the stress redistribution depends on the distance to the broken fibre. As cluster formation is considered to be the mechanism that dominates failure, local load sharing is the best strategy to predict the behaviour of fibre reinforced composites under longitudinal tension. The LLS models have different backgrounds, ranging from analytical models [10, 25] to spring element models [17, 18, 21] to fibre bundle models [19, 22] or finite elements models [6, 20]. The different modelling approaches have their own advantages, however, it is currently considered that, although the models are able to predict the strength of the material, the physics of failure, mainly the cluster formation, are not accurately predicted [26, 27]. This discrepancy between experimental

and numerical results can be explained by several factors. Additional experimental data is necessary, not only to define the properties of the constituents, as there is no consensus on the fibre strength stochastic properties, but also on the actual failure process, as it has not yet been possible to conclude whether ultimate failure results from the overall accumulation of fibre breaks and clusters distributed over a volume of material, or from the formation of a critical cluster with a universal size [26]. On the modelling side, drawbacks such as not representing accurate microstructures or disregarding dynamic effects have been pointed out [26, 27].

This work aims to provide additional insight on the damage development in unidirectional fibre reinforced composites under longitudinal tension and understanding the properties that affect this evolution. This is achieved by understanding the properties that affect the stress redistribution around a broken fibre, how the stress fields around a cluster of broken fibres evolve with the cluster size and its influence in the macro behaviour of the material. The results from the Spring Element Model (SEM) [21] are compared with the results from the Progressive Failure Model (PFM) [22], using different functions for stress concentration and ineffective length, to understand the models' capabilities to accurately capture the stress redistribution in the tensile failure of fibre composites

2. Modelling strategies

In this work two very distinct model strategies are used. Firstly, the Spring Element Model [21], a simplified finite element model, that inherently accounts for the effects of the different relevant fibre and matrix material properties on the longitudinal failure of composite materials. Secondly, a Progressive Failure Model [22] is used. This model is based on the chain of bundles approach [13] and uses known Stress Concentration Factor (SCF) and ineffective length functions to capture the stress redistribution around a broken fibre. The latter model is used in this work to understand if the current literature SCF and

ineffective length formulations are able to accurately capture the damage process in longitudinal failure of composite materials.

The SEM is able to accurately capture the stress redistribution after a fibre breaks and the effect of the different properties considered in the model, although using simplified 1D elements. Nonetheless, this model requires the solution of a system of equations at each increment, making it more computationally expensive than the PFM. The latter model uses known functions for stress redistribution and uses a superposition rule to determine the final stress redistribution profiles, which is important when there is interaction between multiple fibre breaks. This approach allows the model to be computationally efficient with reduced computational times.

To more realistically capture the stress redistribution, both models consider a random distribution of fibres. This distribution is generated using a modified version of Melro et al. [28] random fibre generator.

2.1. Spring element model

The SEM was firstly developed by Okabe et al. [18, 29] and later extended to a random distribution of fibres and hybrid composites by Tavares et al. [21]. The latter model is used in this work and is briefly explained in this section.

The SEM consists of longitudinal spring elements, which represent the fibres, connected by transverse spring elements representing the matrix. The generated 2D geometry, with a random fibre distribution, is extruded in the fibre direction therefore creating straight fibres that are divided in elements of length (l^z). The fibres are connected by matrix shear elements, being that the mesh of matrix elements is generated using a 2D Delaunay triangulation algorithm [30]. Considering that the cross section area of the fibre does not change along the spring element the stiffness matrix for the fibre elements is given by [21]:

$$\mathbf{K}_f^e = \frac{A_f^e E_f^e}{l^z} \begin{bmatrix} 1 & -1 \\ -1 & 1 \end{bmatrix}, \tag{1}$$

where A_f^e is the fibre sectional area, E_f^e is the fibre elastic modulus. The superscript e refers to element properties or parameters, which can be different for the different fibres involved. The matrix shear elements stiffness matrix is given by:

$$\mathbf{K}_m = \frac{G_m \left(A_m^{(2)} - A_m^{(1)} \right)}{d \ln \left(A_m^{(2)} / A_m^{(1)} \right)} \begin{bmatrix} 1 & -1 \\ -1 & 1 \end{bmatrix} , \tag{2}$$

where G_m is the matrix shear stiffness, d is the length of the element, which is given by the distance between the centres of the fibres it connects minus the radii of the fibres. $A_m^{(1)}$ and $A_m^{(2)}$ are given by:

$$A_m^{(1)} = \frac{2\pi R_1}{n_1} l^z \quad \text{and} \quad A_m^{(2)} = \frac{2\pi R_2}{n_2} l^z , \tag{3}$$

where R_i and n_i are, respectively, the fibre radius and the number of matrix elements connected to the fibre i.

The simulation is done under isostrain conditions and the strain increment in each iteration is computed to trigger failure of a single fibre element. In each iteration the equilibrium system of equations needs to be solved to obtain the relevant fields.

To simulate the longitudinal failure of composite materials an appropriate failure criterion for the fibres is required. A maximum stress failure criterion is considered, which can be written in its general form as:

$$\frac{\sigma_e}{X_T^e} - 1 < 0 \quad \text{if} \quad \sigma_f > 0 , \tag{4}$$

where σ_e is the fibre element stress and X_T^e is the tensile strength of the fibre element, generated according to an appropriate statistical distribution, e.g., Weibull distribution [31].

The matrix behaviour plays an important role in the tensile failure of composite materials, since this is the constituent that allows stress redistribution to occur after a fibre breaks. This stress-redistribution is affected by both matrix plasticity and damage, as well as fibre-matrix decohesion [20, 32]. The matrix is considered to be linear elastic and perfectly plastic. This behaviour is implemented in the SEM using sequentially linear analysis [33, 34].

In a sequentially linear strategy, the stress-strain diagram can be reproduced by consecutively reducing the shear stiffness (G_i) as well as changing the yield stress of each critical element (τ_i^u). The shear stiffness is reduced in a discrete manner according to:

$$G_{i+1} = \frac{G_i}{\alpha_m} \, , \tag{5}$$

where α_m is a parameter larger than one and that can be controlled by the user, ensuring a control in accuracy versus computational time. A more detailed description of the model is available in Tavares et al. [21].

2.2. Progressive Failure Model

In this section the PFM [22] is briefly reviewed. The model is based on the chain of bundles approach [13] and assumes a RVE with a random distribution of fibres. Similarly to the SEM presented, the fibres are divided into elements of length l^z along their longitudinal direction. Each fibre is denoted with the subscript q, while each plane is denoted with the sub-subscript p. Furthermore, each element has a stochastic strength according to an appropriate statistical distribution. Once an element fails, a damage is distributed over the ineffective length of the broken fibre, whereas stress concentration is applied into the neighbouring intact fibre elements. The stress redistribution is performed according to different analytical formulations, presented in Section 2.2.1 and 2.2.2. The proposed approach allows to capture both fibre clustering and stiffness loss of composite materials under longitudinal tension.

The constitutive equation of the PFM which relates the stress of each element, $\sigma_{p,q}$, and the strain ε_p is

$$\sigma_{p,q} = \frac{SCF_{p,q}}{\Omega_p} E_f \left(1 - D_{p,q}\right) \varepsilon_p \, , \tag{6}$$

where $SCF_{p,q}$ is the stress concentration factor of element p, q and $D_{p,q}$ is the state damage variable which is equal to 1 for broken elements, equal to zero for intact elements and in between for elements in any stress recovery region. ε_p is the strain of the plane (which is assumed to be the same for all elements of plane p) and Ω_p is a stress ratio which enforces load equilibrium by modifying

the stress concentration according to the strain level. Further details on the load equilibrium scheme can be seen in Guerrero et al. [22]. The evolution of $D_{p,q}$ depends on the formulation for the ineffective length considered while $SCF_{p,q}$ depends on the stress concentration model used. In this work, different formulations for damage and SCF are used in the PFM with the objective of understanding if the current analytical formulations available in the literature can capture accurately the stress redistribution around broken fibres. These formulations are shown in the following sections.

2.2.1. Functions for ineffective length

The stiffness loss of the system is simulated by means of the damage variable, which is obtained using a shear-lag model. Two different possibilities arise depending on the matrix behaviour: perfectly plastic or linear elastic.

If the matrix is assumed to be plastic, the ineffective length $L^{\text{in}}_{p,q}$ of a broken fibre element is computed with the Kelly-Tyson shear-lag model

$$L^{\text{in}}_{p,q} = \frac{E_f R_f}{2\tau^u}\varepsilon_p \ , \tag{7}$$

where τ^u is the shear yield strength of the matrix and R_f is the fibre radius. Another possibility is to use the modified Kelly-Tyson model as given in St-Pierre *et al.* [23], which adds a multiplier factor $H_{p,c}$ that depends on the cluster size, capturing the increase in the ineffective length with the cluster size. Two fibre elements belong to the same cluster (c), if the distance between the centres of both fibres is below four times the fibre radius and both elements are in the same plane p. Thus, at each plane p, there can be several clusters represented by the subscript p, c. The subscript c ranges from 0 to the number of clusters at plane p, N^c_p. With this method, the ineffective length of a broken element belonging to cluster p, c is given by:

$$L^{\text{in}}_{p,q} = \frac{E_f R_f}{2\tau^u} H_{p,c}\varepsilon_p = \frac{n_{p,c}\pi R_f^2 E_f}{C_{p,c}\tau^u}\varepsilon_p \ , \tag{8}$$

where $C_{p,c} = 4s\sqrt{n_{p,c}}$, $n_{p,c}$ is the number of broken fibres on cluster p, c, and s is the mean centre-to-centre distance between each fibre and its closest neighbour, given by $s = R_f\sqrt{\pi/V_f}$, where V_f is the fibre volume fraction.

The damage along the broken fibre within a plastic matrix is simply applied assuming a gradual decrease of damage from 1 at the position of the break, to 0 at both ends of the ineffective length. As fibres may fail many times along their length, different ineffective lengths may overlap. In these cases the highest damage always prevails for each element inside overlapping stress recoveries. Hence an element p, q is affected by each break in the fibre q at each plane i with

$$D_{p,q} = \begin{cases} \max\left(\dfrac{L^{\text{in}}_{i,q} - |i-p|\, l^z}{L^{\text{in}}_{i,q}}\right) & \forall i : (D_{i,q} = 1) \cup \left(|i-p|\, l^z < L^{\text{in}}_{i,q}\right) \\ 0 & \text{otherwise.} \end{cases} . \quad (9)$$

If the matrix is assumed to be elastic, the Cox's [35, 36] shear-lag model is adapted including the same scaling factor $H_{p,c}$ introduced earlier. The scaling factor can also be imposed to be 1, which disables its effect and leads to the original Cox's model. This parameter is added to the model to capture the influence of the cluster size on the ineffective length [23, 24]. The effective stress of a broken element at each plane p due to a break on plane i follows

$$\tilde{\sigma}_{p,q} = E_f \varepsilon_p \left(1 - \exp\left(-\frac{|i-p|\, l^z}{H_{p,c} R_f} \sqrt{\frac{2G_m R_f}{E_f (s - 2R_f)}}\right)\right) , \quad (10)$$

where G_m is the matrix shear modulus. Because the model is exponential, the ineffective length at which the load is completely recovered approaches infinite. This would cause all elements along the length of fibre q to have damage not equal to zero but with an extremely low value. Moreover, no SCF would be applied along the fibre, as the SCF is only applied into elements with zero damage. To avoid having an infinite ineffective length it is here considered the ineffective length to be the distance at which 99.9% of the stress is recovered. Taking this into account, the ineffective length is obtained by substituting $\tilde{\sigma}_{p,q} = 0.999 E_f \varepsilon_p$ in 10:

$$L^{\text{in}}_{p,q} = \frac{-H_{p,c} E_f (s - 2R_f) \ln(0.001) \sqrt{\dfrac{2G_m R_f}{E_f\,(s - 2R_f)}}}{2G_m} . \quad (11)$$

The damage along the ineffective length of the broken fibre can now be

computed by inserting $\tilde{\sigma}_{p,q} = E_f\,(1 - D_{p,q})\,\varepsilon_p$ in Eq. 10 giving

$$D_{p,q} = \begin{cases} \max\left(\exp - \dfrac{|i-p|\,l^z}{H_{p,c}R_f}\sqrt{\dfrac{2G_mR_f}{E_f\,(s-2R_f)}}\right) & \forall i:\,(D_{i,q}=1)\cup\left(|i-p|\,l^z < L_{i,q}^{\text{in}}\right) \\ 0 & \text{otherwise.} \end{cases} . \tag{12}$$

It is worth mentioning that the ineffective length for an elastic matrix does not depend on the strain, ε_p. That is, because the stress transfer in the matrix has no upper limit, whereas it is limited by τ^u in the plastic model.

2.2.2. Functions for stress concentration factor

Different analytical models to predict the SCF around fibre breaks are available in the literature [23, 27, 37]. Here, the SCF is represented within two functions, one depending on the in-plane distance δ and the other which depends on the plane position along the ineffective length λ.

The first option adopted in this work is the model developed by Swolfs *et al.* [27]. This model is based on a micro-mechanical finite element simulation assuming an elastic matrix. The SCF functions for an intact fibre element p, q, around a single broken element i, j are

$$\begin{aligned} \delta_{(q-j)} &= -6.12\ln\left(\frac{d_{q-j}^{\text{c}} - 2R_f}{R_f}\right) + 7.74 \\ \lambda_{(p-i)} &= \exp - \frac{|i-p|\,l^z}{H_{p,c}R_f}\sqrt{\frac{2G_mR_f}{E_f\,(s-2R_f)}} \quad \forall(i,j):\,l^z\,|i-p| < L_{i,j}^{\text{in}} \end{aligned} , \tag{13}$$

where d_{q-j}^{c} is the centre-to-centre distance between fibres q and j.

Similarly, Zhou et al [37] developed a model where the broken fibre contains a debonded and a non-debonded region. The model is used here assuming that no debonding exists. Thus, the functions around a single break are simplified

as

$$\begin{gathered}\delta_{(q-j)} = \frac{2\varphi_{q-j}}{\pi} \\ \lambda_{(p-i)} = \frac{\sinh\beta_j\left(L_{i,j}^{\text{in}} - l^z\left|i-p\right|\right)}{\sinh\beta_j L_{i,j}^{\text{in}}} \quad \forall(i,j) : l^z\left|i-p\right| < L_{i,j}^{\text{in}} \\ \beta_j^2 = \frac{2}{R_f^2 E_f E_{\text{m}}}\left(\frac{E_f\frac{R_f^2}{s^2} + E_{\text{m}}\left(1-\frac{R_f^2}{s^2}\right)}{\frac{1}{4G_f}\left(1-\frac{R_f^2}{s^2}\right) + \frac{1}{2G_{\text{m}}}\left(\frac{s^2}{s^2-R_f^2}\ln\left(\frac{s^2}{R_f^2}\right) - \frac{1}{2}\left(3-\frac{R_f^2}{s^2}\right)\right)}\right)\end{gathered}, \tag{14}$$

where G_f is the broken fibre shear modulus and $\varphi_{q-j} = \arcsin\left(r_j/d_{q-j}^c\right)$. This model also assumes that the matrix is elastic. This model was developed for a 2D composite, however, it is used in a 3D RVE with a random fibre distribution within the PFM framework. This fact may lead to an overestimation of the SCFs, which is further explored in the following sections.

An alternative model was developed by St-Pierre *et al.* [23] where the $SCF_{p,q}$ of an intact fibre around cluster c, located at plane i, is given by:

$$\begin{gathered}\delta_{(q-c)} = I_{i,c}\left(\frac{R_{i,c}}{d_{q-c}^c}\right)^{\alpha} \\ \lambda_{(p-i)} = \begin{cases}\exp -\frac{\left|i-p\right|l^z}{H_{p,c}R_f}\sqrt{\frac{2G_m R_f}{E_f(s-2R_f)}} & \text{Elastic matrix} \\ \dfrac{L_{i,c}^{\text{in}} - l^z\left|i-p\right|}{L_{i,c}^{\text{in}}} & \text{Plastic matrix}\end{cases} \quad \forall(i,c) : l^z\left|i-p\right| < L_{i,c}^{\text{in}}\end{gathered}, \tag{15}$$

where

$$I_{i,c} = \begin{cases}\dfrac{1}{2\ln(R_t/R_{i,c})} & \text{for } \alpha = 2 \\ \dfrac{(2-\alpha)R_{i,c}^{2-\alpha}}{2(R_t^{2-\alpha} - R_{i,c}^{2-\alpha})} & \text{otherwise.}\end{cases}, \tag{16}$$

and $R_{i,c} = s\sqrt{n_{i,c}/\pi}$, $R_t = s\sqrt{N_q/\pi}$ and d_{q-c}^c is the in-plane distance between the centre of the intact fibre p,q and the centre of coordinates of the cluster i,c, whilst $L_{i,c}^{\text{in}}$ is the ineffective length of the cluster, which is equal to the ineffective length of any of the broken elements belonging to the cluster. The value of α is an input parameter of the model, however, according to St-Pierre *et al.* [23], a value of 2 leads to an excellent agreement between the predicted SCF and finite elements when using a plastic matrix.

As there can be multiple breaks or clusters in the model, a superposition rule is considered. The total SCF for an intact fibre is obtained by linear superposition of all broken elements when using the Swolfs and Zhou models, or by linear superposition of the contribution of all clusters when using the St-Pierre model. However, the SCF in a fibre element is bounded according to the capacity of transferring load to the fibre by shear-lag. This limitation enforces a stress continuity between elements inside any ineffective length (elements where $0 < D_{p,q} < 1$) that are not affected by the SCF, and subsequent intact element ($D_{p,q} = 0$) which can be over loaded by the SCF. Thus, the total SCF of an intact element is

$$SCF_{p,q} = \begin{cases} \min\left(SCF^0_{p,q}, SCF^L_{p,q}\right) & \forall p,q:\ D_{p,q} = 0 \\ 1 & \text{otherwise,} \end{cases} , \tag{17}$$

where $SCF^0_{p,q}$ is the SCF predicted by the linear superposition of the contribution of all breaks using the interacting functions as

$$\begin{aligned} SCF^0_{p,q} &= 1 + \sum_{i=1}^{N_p}\sum_{j=1}^{N_q} \delta_{(q-j)}\, \lambda_{(p-i)}\, [D_{i,j} = 1] \qquad \text{Swolfs or Zhou models} \\ SCF^0_{p,q} &= 1 + \sum_{i=1}^{N_p}\sum_{c=1}^{N^c_i} \delta_{(q-c)}\, \lambda_{(p-i)} \qquad \text{Pierre model} \end{aligned} , \tag{18}$$

where here $[\bullet]$ are the Iverson brackets and define 1 if $\bullet$ is true, and 0 if it is false. $SCF^L_{p,q}$ is the SCF limit calculated as the slope defined by the stress gradient of the nearest ineffective length:

$$SCF^L_{p,q} = \min\left(\frac{1}{L^{\text{in}}_{i,q}}\,|i-p|\,l\right) \quad \forall i:\ D_{i,q} = 1\ . \tag{19}$$

3. Methodology

In this study, both the SEM and the PFM use the same representative volume element (RVE) when computing the same problem. The RVE has a dimension of $75 \times 75 \times 300$ fibre radius and considers a random distribution of fibres. A fibre element size of two times the fibre radius was considered in all cases.

For the SEM all the material properties in study are input directly into the model, making it a robust tool, although more computationally expensive.

For the PFM different functions for SCF and ineffective length are used depending on the model properties. Two methods to determine the ineffective length and fibre damage variables are available, depending if the matrix behaviour is plastic or elastic. In the case where a plastic matrix is considered Equations (8) and (9) are used, while for the elastic case Equations (11) and (12) are used. In any of the cases, $H_{p,c}$ can be a function of the cluster size or equal to 1 if this effect is to be ignored. When $H_{p,c}$ is different than 1, the ineffective length scales with the cluster size. Thus, the larger the cluster the larger the ineffective length. However, when $H_{p,c} = 1$, the ineffective length does not scale with the cluster size. This leads to four possible combinations: plastic matrix ($\tau^u \neq \infty$) with cluster scaling ($H_{p,c} \neq 1$) and without cluster scaling ($H_{p,c} = 1$), and elastic matrix ($\tau^u = \infty$) with and without cluster scaling.

Regarding the SCF, three analytical formulations were presented in Section 2.2.2. Zhou's and Swolf's formulations for the SCF consider the matrix to be elastic and are, therefore, used only with the elastic formulation for ineffective length, i.e. with Equations (11) and (12). With St-Pierre's model it is possible to change the SCF function by changing the parameter α. The original authors of the model [23] found a good agreement between the formulation and FEM simulations with a plastic matrix for $\alpha = 2$. This value of α is used in this work for the cases where $\tau^u \neq \infty$, in combination with the plastic formulation for the ineffective length (with or without cluster scaling). To be able to use the latter model with an elastic matrix, the authors adjusted the α parameter to obtain a similar stress redistribution profile to the one obtained with SEM with an elastic matrix. For this case, $\alpha = 3.8$ was found to be a good approximation for an elastic matrix. In the cases where $\alpha = 3.8$ is considered, the elastic formulation for the ineffective length is always used.

To understand the properties that affect the stress redistribution around a broken fibre, an in-depth study is done. This study focuses on the effects of material properties, such as fibre elastic modulus and matrix shear modulus,

on the stress fields around broken fibres. To quantify the stress redistribution profile three metrics are studied. Firstly, the SCFs in the intact fibres that surround a broken one are analysed. The SCF is defined here as the ratio of the actual stress in an intact fibre over the stress if there were no breaks, given by $E_f\varepsilon$, where ε is the applied strain. To have a comparable metric between the cases in study, the maximum SCF (SCF_{max}) is analysed, which is the maximum of the SCFs in all the intact fibres that surround the broken one. Secondly, the ineffective length (L^{in}), which is the region of the broken fibre that looses stress carrying capacity after that fibre breaks, is also analysed. The ineffective length is here considered to be the distance from the break plane that the broken fibre regains 90% of its stress carrying capacity. Lastly, the radial influence length (R^{inf}) is also analysed. This is defined as the maximum distance in the break plane between the broken fibre and an intact fibre that has a stress concentration higher than 1% (SCF$>$ 1.01). In the presented results, both the ineffective length and radial influence length are normalized by the fibre radius R_f.

To understand the influence of the different parameters on the tensile behaviour of the material, different cases are simulated under fibre tensile loading. For this purpose, randomly generated strength, based on the Weibull distribution [31], is assigned to each fibre element, using the element size for length scaling. This is done by generating a random failure probability for each element, which is then converted into a respective element strength. Different metrics are proposed to compare the results between cases and models. These metrics are the strength (defined as the maximum stress reached by the material), the cluster size at maximum stress and the fibre break density at maximum stress.

The following sections are organized as follows. Firstly the stress fields around a single break are analysed. The SEM is used to understand what are the main properties affecting the stress redistribution and these results are then compared with the analytical formulations presented. Afterwards, cluster growth is analysed and its effect on the stress redistribution metrics is studied.

Finally, the material's tensile behaviour is analysed for the different models and the results are correlated with the different stress redistribution profiles.

4. Stress fields around a single broken fibre

In this section the stress fields around a single broken fibre are analysed, with focus in understanding the material properties that affect the stress redistribution and how the analytical formulations accurately capture these fields.

4.1. Factorial design definition

In the spring element model, the stress redistribution depends not only on the elastic and strength properties of the constituents, but also on the actual random arrangement of fibres. To study the effect of each individual property on the stress redistribution, as well as eventual interactions between them, a factorial design of experiments is made.

After a preliminary analysis on the main influencing factors on the stress redistribution, the factors that are considered in this study are the fibre elastic modulus (E_f), the matrix shear modulus (G_m) and strength (τ^u), the fibre volume fraction (V_f) and the fibre radius (R_f). As the SEM is able to take into account all these factors, the factorial analysis will be done in that model and later compared with the analytical stress distribution functions used in the PFM.

To study the effects of the different parameters it is necessary to define levels for these parameters. For all the parameters, with exception of the matrix shear strength, it was decided that two levels are enough for this study. For the matrix shear strength it was decided that three levels would be used, two finite levels and a third considering the matrix to be elastic ($\tau^u = \infty$). Table 1 shows the different parameters and the levels that were assigned to them.

With the proposed factors and respective levels, there are forty-eight ($48 = 3^1 2^4$) cases to study. Due to the random nature of the fibre distribution, that affects the stress redistribution around a broken fibre, ten calculations, with

Table 1: Parameters and respective levels used in this study

Factor		Level		
		0	1	2
A	E_f (GPa)	70	230	-
B	G_m (MPa)	450	1050	-
C	τ^u (MPa)	50	100	∞
D	V_f	0.4	0.6	-
E	R_f (μm)	3.5	7.0	-

different geometries, were done for each case that were averaged to get the necessary parameters for the sensitivity analysis. The results presented are obtained considering a remote applied strain of 2%.

4.2. Spring element model results

Table 2 shows the average results and coefficients of variation for the factors and metrics in study. The values presented are the average of all the cases at each level of the respective factor. This means that any effects of all other factors on this average are disregarded. The coefficients of variation are also shown in this table. It should be noted that both the ineffective length (L^{in}) and the radial influence length (R^{inf}) are in the normalised form, as they are divided by the fibre radius (R_f).

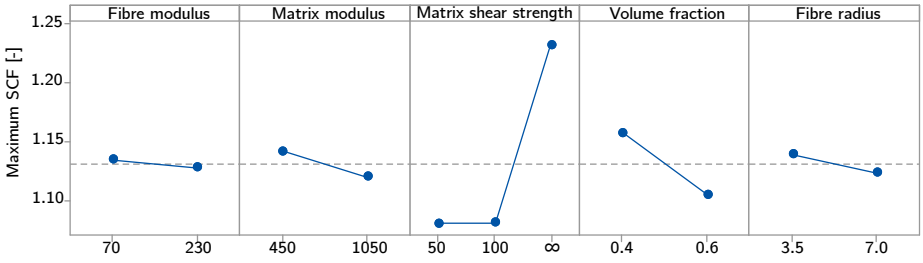

Figure 1: Main effects plot for the maximum SCF.

Figures 1 and 2 show, respectively the influence of each parameter, at each

Table 2: Average results obtained with the proposed factorial design.

Factor	Level	SCF_{max}		L^{in}		R^{inf}	
		Avg. (-)	CoV (%)	Avg. (-)	CoV (%)	Avg. (-)	CoV (%)
E_f (GPa)	70	1.134	6.3	13.775	27.8	4.299	11.8
	230	1.127	8.2	31.475	34.9	4.247	17.2
G_m (MPa)	450	1.141	7.2	24.742	49.8	4.204	14.0
	1050	1.119	7.3	20.508	57.1	4.342	15.2
τ^u (MPa)	50	1.079	2.4	27.138	45.5	4.474	13.2
	100	1.080	2.5	26.650	45.3	4.455	13.2
	∞	1.232	4.6	14.088	46.5	3.890	13.7
V_f	0.4	1.157	7.8	25.075	47.6	4.723	9.5
	0.6	1.104	5.8	20.175	59.4	3.822	10.7
R_f (μm)	3.5	1.138	8.3	21.850	54.6	4.024	14.2
	7	1.123	6.0	23.400	53.2	4.521	12.9

level, on the maximum SCF and the Pareto front for standardized effects on the maximum SCF. The Pareto chart shows the effect that each factor has on the analysed property. The ones whose standardized effect is larger that 2.05 (red line) are statistically representative. From the analysis of the data it is concluded that the main factors affecting the maximum SCF are the fibre volume fraction (V_f), the matrix shear strength (τ^u) and the matrix shear modulus (G_m). Similarly to what was shown in the work of Swolfs et al. [11] for an elastic matrix, an increase in the fibre volume fraction leads to a reduction in the maximum SCF. It is interesting to note that the fibre elastic modulus (E_f) has a small effect on the maximum SCF. Another point to note is that the matrix shear strength not only affects directly the SCF but also has a combined effect with other properties such as the fibre modulus (AC) and the fibre radius (CE). This makes the matrix shear strength the most important factor affecting the SCF. Analysing Figure 1 it is possible to see that changing the matrix shear strength from 50 to 100 MPa doesn't have an important effect on the SCF.

On the other hand, considering the matrix to be linear elastic ($\tau^u = \infty$) has a large effect on the maximum SCF: from $SCF_{max} = 1.08$ for $\tau^u = 50$ MPa to $SCF_{max} = 1.23$ for $\tau^u = \infty$. This high difference between considering the matrix elastic perfectly plastic and linear elastic also occurs in the combined factors AC and CE, which underlines the importance of the matrix shear stress on the predicted stress concentration factors.

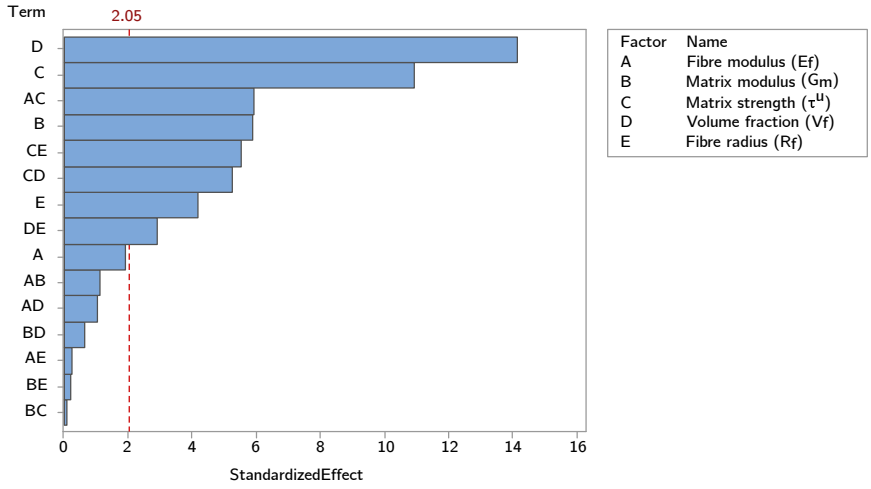

Figure 2: Pareto chart of the standardized effects on the maximum SCF.

Regarding the ineffective length, the most influential factor is the fibre elastic modulus. This can be explained by the fact that, with a higher fibre modulus, the stress that needs to be transferred back to the fibre by shear in the matrix is higher and, therefore, so will be the ineffective length. It should be noted that for this analysis a constant applied strain of 2% was used and, therefore, different fibre stress depending on the fibre modulus. If a constant fibre stress was considered, the higher fibre modulus would lead to higher shear stress in the matrix and, therefore a reduced ineffective length[10]. The ineffective length is affected by the ability of the matrix to transfer the stress back to the broken

fibre. This means that it will also be affected by the matrix modulus and the matrix shear strength. The matrix shear modulus directly affects the ineffective length, however, the matrix shear strength affects the ineffective length not only directly but also as a combination with the fibre elastic modulus, similarly to what occurred in the SCF analysis. The fibre volume fraction also has an important effect on the ineffective length, being the second parameter that most affects this property. With a higher fibre volume fraction the ineffective length is reduced, as the homogenized stiffness of the material that surrounds the broken fibre is higher and, therefore, it is easier for the broken fibre to recover its load carrying capacity. This is specially true if $\tau^u = \infty$ as there is no limit in the shear stress that the matrix can withstand. Nevertheless, it should be noted that fibre-matrix debonding was not considered in any of the presented models, which has been shown to increase the ineffective length [38].

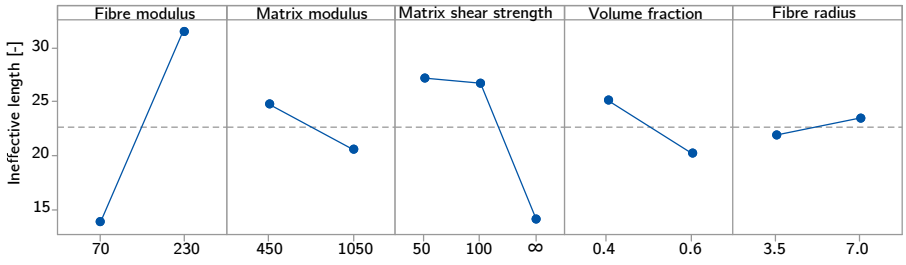

Figure 3: Main effects plot for the ineffective length.

The radial influence length (R^{inf}) is a factor that measures the radial distance in the break plane that is affected by the broken fibre. This distance is highly dependent on the actual fibre arrangement that surrounds the broken fibre. The radial influence length is a parameter that strongly depends on the local fibre arrangement. It was seen that for the same case there was a very high variability of this metric, which makes it difficult to conclude about the most influencing factors. Nonetheless, it is seen that the radial influence length depends more on the volume fraction and on the matrix shear strength, being higher when the matrix is considered linear elastic ($\tau^u = \infty$), as the maximum

SCF is also higher.

4.3. Model comparison

In Section 2.2 different analytical models for the stress concentration factor and ineffective length have been presented. In this section the results from the SEM are compared with the analytical formulations and the validity of each approach is discussed. The RVEs used in the SEM and PFM are the same as in the previous study. The values shown are for a fibre volume fraction of 60%, a fibre radius equal to 3.5 μm and an applied strain equal to 2%.

4.3.1. Ineffective length

Table 3 shows a comparison between the results obtained using the SEM and the respective analytical formulations. Regarding the analytical formulations, when $\tau^u = \infty$, the ineffective length is computed using Equation 11, else it is done so using Equation 8. Note however, that Equation 8 returns the ineffective length at 100% of load recovery while Equation 11 returns the ineffective length at 99.9% of load recovery. Here the results shown are for 90% of load recovery. If cluster scaling is considered, the ineffective length is multiplied by the factor $H_{p,c}$ that, for a single fibre break, $V_f = 60\%$ and $R_f = 3.5$ μm, is equal to 0.7625. The results for the ineffective length are shown in the normalized form, therefore, the ineffective length is divided by the fibre radius.

The analytical formulations overall capture similar ineffective lengths as the SEM, if no cluster scaling is considered ($H_{p,c} = 1$). However, if $\tau^u \neq \infty$ is considered, while the SEM results depend on the matrix shear modulus, the analytical formulations do not. In the case of an elastic matrix ($\tau^u = \infty$) this dependency is well captured, being the results from the SEM very similar to the analytical formulation. If cluster scaling is considered, then the ineffective length is reduced, but the variances are the same as if no scaling is considered. It is interesting to note that for $E_f = 70$ GPa and $\tau^u = 50$ and 100 MPa, the ineffective length for the SEM does not change, while it changes using the analytical formulations. This difference is attributed to the fact that the analytical

Table 3: Ineffective length comparison of the SEM and the various PFM analytical formulations. The average of 10 realisations is shown.

E_f (GPa)	G_m (MPa)	τ^u (MPa)	SEM	PFM	
				$H_{p,c}=1$	$H_{p,c}\neq 1$
70	450	50	15.0	12.6	8.6
		100	15.0	6.3	4.3
		∞	9.6	10.9	7.5
	1050	50	13.0	12.6	8.6
		100	12.4	6.3	4.3
		∞	6.8	7.1	4.9
230	450	50	38.4	41.4	28.4
		100	37.4	20.7	14.2
		∞	16.4	19.8	13.6
	1050	50	35.2	41.4	28.4
		100	34.8	20.7	14.2
		∞	11.2	12.9	8.9

models considered the matrix to be perfectly plastic, while the SEM considered the matrix elastic perfectly plastic. Similar results were found for a fibre radius of 7.0 μm and are not shown here.

4.3.2. Stress concentration factor

In Section 2.2.2 different analytical formulations for the SCF in the intact fibres that surround a broken one were presented. These formulations are based on different assumptions and, therefore, will result in different SCFs. Table 4 shows the maximum SCF results of the different analytical formulations as well as results using SEM for different cases. These cases were formulated taking into account the most influencing factors in Section 4.2. For the SEM, results are shown for different matrix shear strengths. Similarly, using St-Pierre's model, different values for α are used. $\alpha = 2$ for a plastic matrix [23], while $\alpha = 3.8$ was chosen for an elastic matrix as the SCF distribution function has a good agreement with the SEM with $\tau^u = \infty$.

Table 4: Maximum stress concentration factor of the SEM and the various PFM analytical formulations. The average of 10 realisations is shown.

V_f	E_f (GPa)	G_m (MPa)	SEM $\tau^u =$ 50	SEM $\tau^u =$ 100	SEM $\tau^u =$ ∞	PFM Swolfs	PFM Zhou	PFM St-Pierre $\alpha =$ 2	PFM St-Pierre $\alpha =$ 3.8
0.4	70	450	1.127	1.127	1.315	1.205	1.309	1.082	1.287
		1050	1.095	1.096	1.285	1.205	1.309	1.082	1.287
	230	450	1.093	1.093	1.341	1.237	1.319	1.087	1.319
		1050	1.071	1.072	1.324	1.237	1.319	1.087	1.319
0.6	70	450	1.083	1.083	1.193	1.26	1.324	1.056	1.155
		1050	1.061	1.061	1.168	1.26	1.324	1.056	1.155
	230	450	1.060	1.061	1.218	1.252	1.322	1.0558	1.152
		1050	1.044	1.044	1.202	1.252	1.322	1.0558	1.152

The SEM captures the changes in stress redistribution from all the parameters that affect the model. On the contrary, the analytical formulations are not able to do so. For instance, none of the models captures the changes in the SCF with the matrix shear modulus. Regarding the effect of the fibre volume fraction on the SCF, all models capture some change with this parameter. In the case of Swolfs and Zhou's models, this effect is captured due to a change in the distance between the fibres, however, St-Pierre's model directly depends on the fibre volume fraction. On average, the lower the volume fraction, the higher the SCF should be [11]. This is captured by the SEM as well as St-Pierre's formulation. However, with Swolfs and Zhou's models the SCF increases with increasing the volume fraction, as the fibres are closer together and, therefore, the distance between them is smaller. This difference in trend can be explained by the fact that Zhou's and Swolfs' models consider that there is a direct dependency between the inter fibre distance with the volume fraction, which is not the case in randomly distributed fibres. For lower volume fractions, the stress from the broken fibre is redistributed mainly to the closest fibre, as the fibres are further apart, while for higher volume fractions the stress is more

evenly redistributed among the neighbouring intact fibres. Regarding the effect of the fibre elastic modulus, it was shown in Section 4.2 that this parameter did not highly influence the SCF, but did so when combined with the matrix shear strength. None of the analytical formulations capture directly this effect. From the results, it is possible to see that Swolfs and Zhou's formulations give similar results to the SEM with $\tau^u = \infty$ and St-Pierre's model with $\alpha = 3.8$, which represent an elastic matrix. For the case of a plastic matrix, the results from SEM and St-Pierre's model are in good agreement, disregarding the changes in the SCF with the value of the matrix shear modulus. It should be noted that, although Swolfs' and St-Pierre's models do not capture directly the effects of several parameters, finite element simulations can be used to calibrate the SCF functions for each material.

The radial influence length was not included in this study as it was similar in all the presented models.

5. Multiple fibre break analysis

In this section, the effects of fibre break clustering on the stress redistribution are studied. As the interaction between the fibre breaks and cluster formation is considered to be the basis of the failure of composite materials, it is important to understand how the stress redistribution changes with an increase in cluster size. To understand this effect, the models presented were used to study the effects of cluster size on the maximum SCF, ineffective length and radial influence length. To do so, a RVE with a random distribution of fibres with radius equal to 3.5 μm and a fibre volume fraction of 60% was considered. The fibres were considered to have a modulus equal to 230 GPa, which is representative of carbon fibres. From this RVE 10 fibres were selected randomly to initialize the cluster formation. A remote tensile strain of 2% is applied. To simulate the cluster formation, after each break, the next fibre with the higher SCF is broken, leading to an increase in the number of broken fibres in the cluster and changes in the stress redistribution. It should be noted that the path of cluster growth is not known

a priori and different models may lead to different cluster shapes with the same number of broken fibres.

The ineffective length of a cluster was considered to be the largest ineffective length of the individual broken fibres that are part of that cluster, being here considered the length at which the fibre recovers 90% of its load carrying capacity. The analytical formulations presented in section 2.2.1 were used in the PFM, and are independent on the model for SCF used. The results for the ineffective length are shown in the normalized form the ineffective length is divided by the fibre radius.

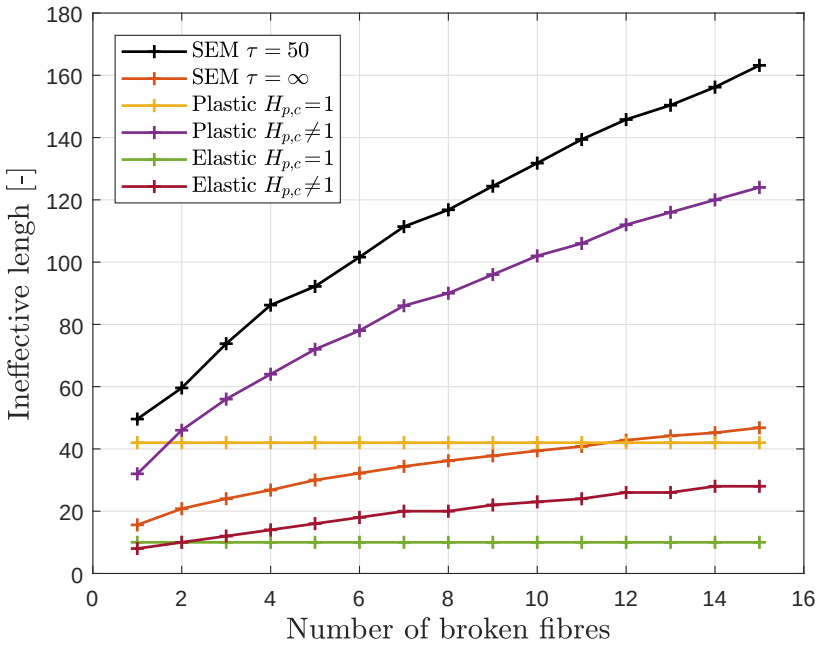

Figure 4: Effect of the cluster size on the ineffective length. The average of 10 realisations is shown.

As shown in Figure 4, the formulations for the ineffective length that use the base Kelly-Tyson (plastic $H_{p,c} = 1$) and Cox (elastic $H_{p,c} = 1$) models do not scale with the number of broken fibres. This drawback can, however, be solved by using the size cluster scaling proposed by St-Pierre et al. [23, 24], i.e.

$H_{p,c} \neq 1$. For both cases, elastic and plastic matrix, the scaling trend is similar to that obtained with the SEM. The ineffective lengths obtained with the SEM are, however, always larger than those predicted by the analytical simulations, being the difference larger for larger cluster sizes. Nonetheless, it should be noted that some differences in the ineffective length may be due to the different cluster shapes formed with the different models.

Figure 5 shows the scaling of the maximum SCF as a function of the number of broken fibres within a cluster. In addition to the results from the SEM and PFM models, the analytical solutions proposed by Hedgepeth [10] for 2D and Hedgepeth and Van Dyke [25] for a 3D hexagonal fibre arrangement are also shown.

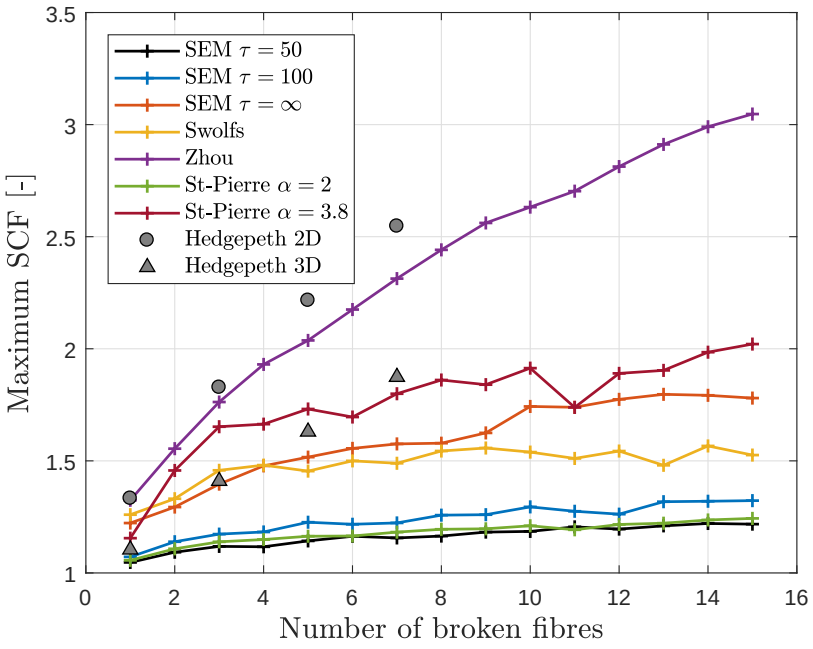

Figure 5: Effect of the cluster size on the maximum SCF. The average of 10 realisations is shown.

As expected, all models are able to capture the increase in SCF due to the increase in the number of broken fibres. This can be expected as there

is additional stress that needs to be redistributed due to the increase in the number of broken fibres. Nonetheless, the different models have different trends. Zhou's model predicts the highest SCF for a single break, a trend that scales with the increase in broken fibres, reaching values of maximum SCF over 3. This value is considered too high as unstable propagation of the cluster should occur before this SCF level is reached. Nonetheless, it should be noted that this model is based on a 2D planar fibre arrangement and, therefore, leads to an overestimation of the SCFs in a 3D composite. The remaining models have a much lower scaling with the number of broken fibres, being that for St-Pierre's model, the SCF functions directly depend on the number of broken fibres. Comparing the models that consider the matrix plastic (SEM $\tau^u = 50$, SEM $\tau^u = 100$ and St-Pierre $\alpha = 2$), it is possible to see that all the models give very similar results, with a low scaling of the maximum SCF. The moderate increase in the maximum SCF is due to the fact that the matrix is not able to transfer more stress to the closest fibres, due to the shear stress limit, therefore, this stress needs to be redistributed to fibres further away from the cluster, not affecting the maximum SCF. When the matrix is considered elastic (SEM $\tau^u = \infty$, Swolfs, Zhou and St-Pierre $\alpha = 3.8$), the stress redistribution is more local and, therefore, the maximum SCF has a more pronounced increase with the number of broken fibres. In this case, the SEM has a similar trend as Swolfs' model, being that the SEM has lower SCF for small clusters and higher for the larger clusters (see Figure 5). St-Pierre's model, in this case, predicts a large increase on the SCF from a single broken fibre to a cluster of two broken fibres, being the increase in SCF with each additional fibre reduced for larger clusters. Interestingly, there is a decrease in the maximum SCF for a cluster of 11 fibres. For different models, it is possible to see that there is a decrease in SCF when the number of broken fibres increases. This should be a consequence of the random fibre arrangement. Comparing the results from the SEM and PFM with the analytical solutions by Hedgepeth [10, 25], it is possible to see that Zhou's model is in good agreement with Hedgepeth as both are based in a 2D planar arrangement of fibres. The 3D solution shows a similar scaling

as the remaining models, however, it should be noted that while the analytical formulation is for a periodical hexagonal arrangement of fibres, the results from the SEM and PFM are for a random distribution of fibres.

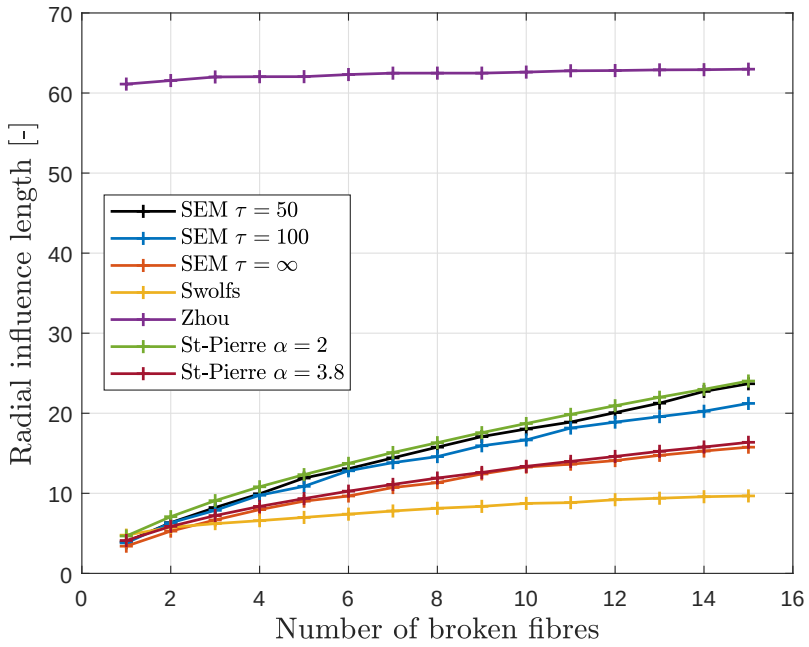

Figure 6: Effect of the cluster size on the radial influence length. The average of 10 realisations is shown.

The radial influence length is the distance in the failure plane that is affected by more than 1% of stress concentration. This distance, for the cases with more than one broken fibre, was measured to the geometrical centre of the cluster. Figure 6 shows the scaling of the radial influence length with the number of broken fibres within a cluster. All models predict an increase in the radial influence length with an increase in cluster size, as expected. Zhou's model has a much higher radial influence length that scales less with the cluster size. This is due to the nature of the SCF function, whose shape causes a large region surrounding the broken fibres to have a SCF higher than 1%, which was the value used to limit the radial influence length. The other models have a very

similar radial influence length for a single broken fibre, between 3.8 and 4.8 times the fibre radius. However, the models scale different with the increased cluster size. Swolfs' model predicts a lower scaling in radial influence length as the matrix is considered elastic. Similarly, the SEM and St-Pierre models show a lower increase in radial influence length for the elastic case ($\tau^u = \infty$ and $\alpha = 3.8$). Both the SEM and St-Pierre models show very similar scaling of the radial influence length with the cluster size for both the elastic and plastic cases. The similarity between these two models can also be observed for the other parameters studied, namely the maximum SCF.

6. Tensile behaviour

In this section, a comparison between the several models is done at the RVE scale with the objective of understanding how the differences in the local stress fields affect the tensile behaviour and cluster formation.

To understand these effects, the same study was done in two types of fibres, one carbon fibre and one glass fibre. The variance of three factors was studied for each type of fibre. The factors selected are the matrix shear modulus (G_m), the matrix shear strength (τ^u) and the fibre volume fraction (V_f), as they affect the stress redistribution the most (Section 4.2). For the matrix shear modulus and volume fraction the same levels as in Section 4.2 were explored, however, for the matrix shear strength only two levels were considered: $\tau^u = 50$ MPa and $\tau^u = \infty$. The third level was removed as the effects of changing the shear strength from 50 to 100 MPa were reduced. A full factorial study was performed with a total of eight cases for each type of fibre. For each case five simulations were performed. The fibre strength is assigned to each fibre element randomly with a Weibull distribution. The Weibull properties (σ_m, m and L_0) and the remaining material parameters are shown in Table 5.

Table 6 shows the summary of the average results of 10 simulations for the different models with distinct input parameters. In this section, and similarly to other works in the literature [19, 21], two fibres are considered to be in the

Table 5: Fibre properties used for RVE study [17, 39].

Fibre	R_f (μm)	E_f (GPa)	σ_0 (MPa)	m	L_0 (mm)
Carbon	3.5	234	4275	10.7	12.7
Glass	7.0	70	1550	6.34	24

same cluster if their centres are within four times the fibre radius and the fibre break planes are within ten times the fibre radius in the longitudinal direction. The tensile strength (X_t) is calculated by means of the rule of mixtures.

Table 6: Carbon RVE simulation results for different models and parameters. The average of 10 realisations is shown.

			SEM			St-Pierre			Swolfs			Zhou		
V_f	τ^u (MPa)	G_m (MPa)	X_t (MPa)	Max. cluster	Break density (/mm^3)	X_t (MPa)	Max. cluster	Break density (/mm^3)	X_t (MPa)	Max. cluster	Break density (/mm^3)	X_t (MPa)	Max. cluster	Break density (/mm^3)
0.4	50	450	1784	5.4	2228	1923	11.2	5045	-	-	-	-	-	-
		1050	1802	6.0	2809	1954	18.4	5169	-	-	-	-	-	-
	∞	450	1844	9.8	3184	1646	2.4	586	1963	20.0	7151	1810	4.4	1833
		1050	1921	11.2	4708	1778	4.0	1200	2050	43.2	9291	1834	3.6	1706
0.6	50	450	2698	4.4	3696	2843	8.2	6925	-	-	-	-	-	-
		1050	2718	5.8	4600	2856	18.4	7328	-	-	-	-	-	-
	∞	450	2911	11.4	6994	2695	7.8	2482	2859	14.2	5440	2585	2.8	1526
		1050	2952	6.6	7331	2828	13.6	3630	2978	20.6	8229	2598	3.2	1446

Figure 7 shows the results for the different models and cases where the matrix is considered linear elastic ($\tau^u = \infty$). For a constant fibre volume fraction the difference in strength predicted by the different models is small and all of them predict accurately the increase in strength (X_t) with the increase in fibre content. The change in the matrix shear modulus has only a small effect in the predicted strength, but all models predict an increase in the strength with the increase in matrix shear stiffness. It should be noted that all predicted strengths are high, compared to typical composite material strengths. This is due to the fact that the Weibull distribution is scaled to very small lengths (7 μm) which

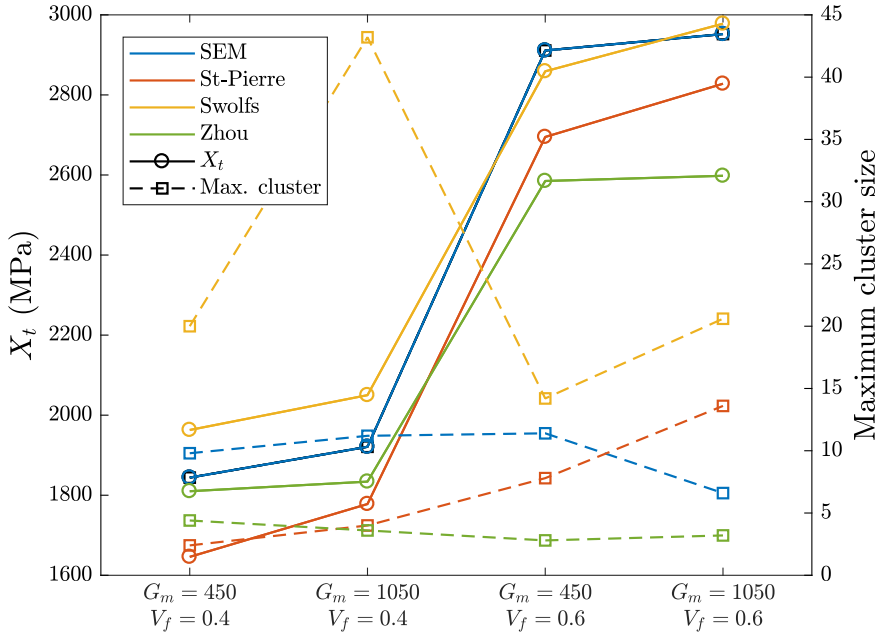

Figure 7: Tensile strength and maximum cluster size for the elastic matrix cases ($\tau^u = \infty$) for carbon fibre. The average of 10 realisations is shown.

leads to very high element strengths. This leads to an overprediction of the strengths [21, 27, 38, 39]. Additionally, the RVE analysed has a small volume compared to that of a typical specimen used to characterize composite material strengths. Due to the size effects present in composite materials [38, 40], care must be taken when comparing the numerical results with experimental ones. Nonetheless, the comparison between the results of the different models should not be affected by this fact, as similar strategies to generate the strength of the elements were used.

Regarding the maximum cluster size, with exception of Swolfs' model, all models predict similar critical cluster sizes in all cases. In Swolfs' model, the maximum predicted cluster size is 43 fibres, which is a very high value compared with the data available in the literature [4, 19, 21]. Similarly, the models predict a very high fibre break density at peak stress, which is not seen in the available

experimental data [4, 19].

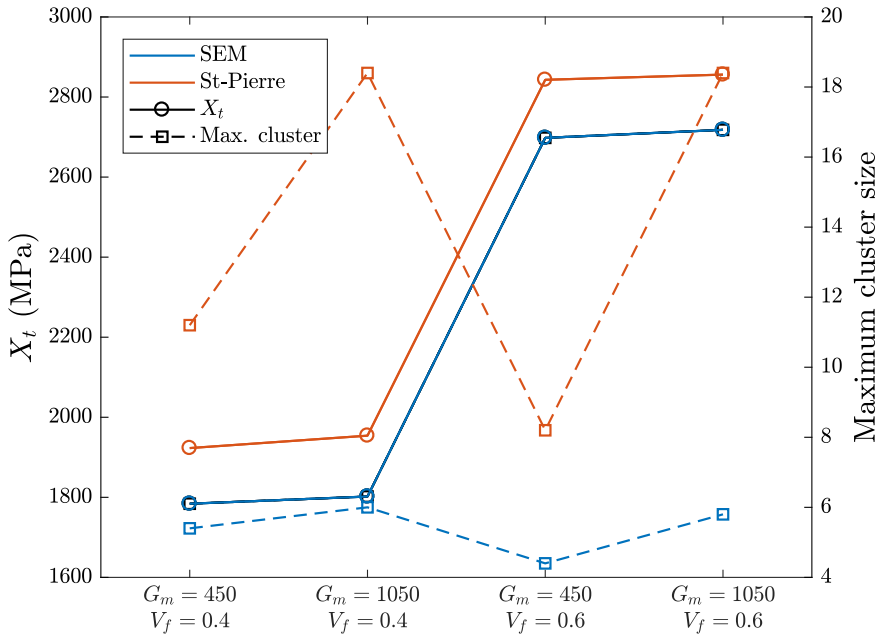

Figure 8: Tensile strength and maximum cluster size for the plastic matrix cases ($\tau^u = 50$) for carbon fibre. The average of 10 realisations is shown.

Figure 8 shows the predicted strength and maximum cluster size for the cases where the matrix is considered plastic. These results are only available for the SEM and St-Pierre's model. Both the SEM and the PFM with St-Pierre's SCFs have the same trends, being the predicted cluster size higher for St-Pierre's model.

It is interesting to note that the trends observed, in moving from an elastic to a plastic matrix, with the SEM and St-Pierre's models are very distinct (Table 6). While for the SEM the maximum cluster size and the strength are lower when the matrix is considered plastic ($\tau^u = 50$ MPa), with the other model the opposite happens. With PFM it is seen that the material strength obtained is lower in the elastic case than in the plastic case and so is the predicted maximum cluster size. Similarly, the fibre break density at peak stress is lower in the elastic

cases for St-Pierre's model, while it is lower in the plastic cases for the SEM.

Analysing the evolution of the SCFs as a function of the cluster size (Figure 5) it is possible to see that for St-Pierre's model the SCF increases rapidly for a small cluster size when the matrix is considered elastic. This rapid increase leads to the earlier formation of clusters of higher dimensions. In addition the authors observed that the formation of cluster of 3-4 fibres leads to the failure of the material, therefore, resulting in a lower strength and failure strain. With the SEM this increase is more gradual and always with lower SCF, for clusters with more than a broken fibre. This explain the premature failure predicted by St-Pierre's formulation when $\alpha = 3.8$, e.g. elastic matrix, is considered. Nonetheless, it should be noted that this can be avoided by adjusting the α for several cluster sizes instead of adjusting it to accurately capture the stress fields around a single break, as was done for $\alpha = 3.8$.

Similarly to what was done for carbon fibre, Table 7 shows the influence of several material parameters on the tensile behaviour of composite materials. In this case glass fibres are used, whose properties are shown in Table 5. Similar trends are found between the glass and carbon cases. All modelling strategies are able to capture the increase in tensile strength with the volume fraction. For the SEM there is also a increase in the tensile strength if the matrix is considered elastic and if the matrix shear modulus is increased. The same effect of the matrix shear modulus is seen in the remaining models. However, similarly to what occurred for the carbon cases, with St-Pierre's model, there is a decrease in the strength in the cases where the matrix is considered linear elastic. Again this is in contrast with the results obtained with the SEM. However, in this case the maximum cluster size predicted with St-Pierre formulation is higher in the elastic cases than in the plastic cases.

Regarding the maximum cluster size it is seen that the predicted cluster size is overall higher than for the carbon cases, which is expected as there is a higher dispersion in the strength of glass fibres (lower Weibull modulus m). However, for the cases where the matrix is elastic the values for the maximum cluster size are very high, sometimes higher than the total number of fibres in the RVE. In

Table 7: Glass RVE simulation results for different models and parameters. The average of 10 realisations is shown.

			SEM			St-Pierre			Swolfs			Zhou		
G_m (MPa)	τ^u (MPa)	V_f	X_t (MPa)	Max. cluster	Break density (/mm^3)	X_t (MPa)	Max. cluster	Break density (/mm^3)	X_t (MPa)	Max. cluster	Break density (/mm^3)	X_t (MPa)	Max. cluster	Break density (/mm^3)
0.4	50	450	810	14.8	2387.0	938	24.4	2550.1	-	-	-	-	-	-
		1050	817	29.8	2637.8	974	61.8	2590.8	-	-	-	-	-	-
	∞	450	917	517.2	7694.4	909	291.2	3503.0	1010	247.0	5329.5	870	11.4	1344.8
		1050	964	1311.2	10240.3	968	450.4	4529.3	1108	1018.6	7631.5	921	17.0	1444.3
0.6	50	450	1233	57.6	3566.6	1350	103.0	3598.4	-	-	-	-	-	-
		1050	1241	56.0	3479.5	1375	78.0	3436.0	-	-	-	-	-	-
	∞	450	1471	62.5	4870.7	1462	585.6	7004.0	1507	733	7294	1280	23.8	1744.3
		1050	1524	70.0	5477.6	1549	1017.6	9252.1	1616	2109	10223	1329	20.0	1734.6

these simulations two fibres were considered to be in the same cluster if their in-plane distance was lower than four times the fibre radius and the break plane distance lower than ten times the fibre radius. As the fibre radius of the glass fibres was considered twice the one from carbon, the volume considered for two fibres to belong in the same cluster is larger. On the contrary, the ineffective length of the glass fibres are lower due to the lower fibre elastic modulus. This makes it possible for the same fibre to break more than once in the region considered for the cluster and, therefore, overpredicting the cluster size. This factor makes it necessary to have a better definition of a cluster of broken fibres, as in some cases, the current definition [4, 19, 21] leads to erroneous results.

7. Conclusions

In this work an extensive analysis on the stress fields and stress redistribution due to fibre failure in fibre reinforced composites under longitudinal tension was performed. The results from a spring element model were compared with the results from a progressive damage model, also with a random fibre distribution, with different ineffective length and stress concentration factor formulations.

An analysis of the effects of the main model input parameters on the stress

fields around a broken fibre was performed using the SEM. From this study it was possible to conclude that different materials with different input parameters, such as fibre modulus, matrix shear stiffness and matrix yield strength, leads to very distinct stress redistribution profiles. In this study three parameters were analysed: maximum stress concentration factor, ineffective length and radial influence length. These parameters were considered to define the stress field surrounding a broken fibre. It was observed that the maximum SCF depends on different input parameters, the most critical being the fibre volume fraction. In addition, it was observed that the matrix yield strength has a large influence on the maximum SCF, mainly when the matrix is considered elastic or plastic. Interestingly, it was seen that the fibre modulus did not have a high effect on the SCF, however, the combination between the fibre modulus and the matrix yield strength affects the SCF. As for the ineffective length, it was seen that the fibre modulus as well as the matrix yield strength were the most influencing factors on this property. Regarding the radial influence length, it was observed that there was a small variation with different input parameters, however, it was found that there was a large variation depending on the local fibre arrangement.

Comparing the results from the SEM with the results from the analytical formulations used within the progressive failure model framework, it is concluded that most models do not capture the dependency of the input parameters on the stress redistribution profile. In most cases, fitting is necessary to obtain accurate stress redistribution functions and, therefore, care must be taken when considering the same SCF function for different materials. It was also seen that there is a large difference between considering the matrix linear elastic or elasto-plastic.

The stress fields that surround a cluster of broken fibres were also analysed. The different models have different evolutions of the maximum SCF, ineffective length and radial influence length as a function of the cluster size. In general, in the models where the matrix was considered linear elastic, the maximum SCF increases more rapidly with the number of broken fibres and the ineffective length has a smaller increase, when compared with the models that consider

the matrix plastic. It should be noted that several models do not consider the increase in ineffective length with the cluster size, however, it was seen that the cluster size has a large effect on the ineffective length, as previously shown in St-Pierre et al. [23, 24]. Adding a factor that scales with the cluster size leads to similar results between the analytical formulations and SEM.

For the representative volume element simulations it was shown that the different presented models predicted different strengths. The main difference is between models considering the matrix elastic or elasto-plastic. Using St-Pierre's model for the SCF functions when the matrix was considered elastic ($\alpha = 3.8$) the predicted strength was lower than when the matrix was considered plastic ($\alpha = 2$). However, the results predicted by the spring element model showed the opposite trend. Regarding cluster formation, it was shown that the maximum cluster size is highly dependent on the input properties of the models. Furthermore, it was seen the current used definition for cluster [21, 41] can lead to erroneous results. In the glass cases, there were clusters with more breaks than the number of fibres in the RVE, meaning that the same fibre was broken more than once in the same cluster.

This work aimed at further developing the understanding of the damage propagation and cluster formation in unidirectional composites. It was shown that more understanding on the phenomena that control failure of unidirectional composites under longitudinal tension and more experimental data are needed. Nonetheless, it is important that the models take into account the real material input parameters as well as an accurate representation of the microstructure to better capture the material behaviour. Therefore, care should be taken when using stress concentration factor functions from a different material system.

Acknowledgements

Rodrigo P. Tavares acknowledges the support of the Portuguese Government's Fundação para a Ciência e Tecnologia, under the Grant SFRH/BD/115872/2016. Jose M. Guerrero, Joan A. Mayugo, Josep Costa and Albert Turon acknowl-

edge the financial support from the Spanish 'Ministerio de Economía, Industria y Competitividad' (MINECO) under the projects MAT2015-69491-C3-1-R and TRA2015-71491-R co-financed by the European Regional Development Fund (ERDF). Jose M. Guerrero would also like to acknowledge the predoctoral Grant BES-2016-078270 from the 'Subprograma Estatal de Formación del MICINN' co-financed by the European Social Fund. Fermin Otero gratefully acknowledges the funding of Project NORTE-01-0145-FEDER-000022 SciTech Science and Technology for Competitive and Sustainable Industries, cofinanced by Programa Operacional Regional do Norte (NORTE2020), through Fundo Europeu de Desenvolvimento Regional (FEDER). Pedro P. Camanho gratefully acknowledges the funding of Project PTDC/EMS-PRO/4732/2014, cofinanced by Programa Operacional Competitividade e Internacionalização and Programa Operacional Regional de Lisboa, through Fundo Europeu de Desenvolvimento Regional (FEDER) and by National Funds through FCT - – Fundação para a Ciência e Tecnologia.

References

References

[1] A. S. Argon, Statistical Aspects of Fracture, in: L. J. Broutman (Ed.), Composite Materials: Fatigue and Fracture, Vol. 5, Academic Press, New York, 1974, Ch. 4, pp. 153–190.

[2] J. Lamon, Mécanique de la rupture fragile et de l'endommagement: approches statistiques et probabilistes, Études en mécanique des matériaux et des structures, Hermes Science Publications, 2007.

[3] F. Tanaka, T. Okabe, H. Okuda, I. A. Kinloch, R. J. Young, Factors controlling the strength of carbon fibres in tension, Composites Part A: Applied Science and Manufacturing 57 (0) (2014) 88–94. doi:http://dx.doi.org/10.1016/j.compositesa.2013.11.007.

[4] A. Scott, M. Mavrogordato, P. Wright, I. Sinclair, S. Spearing, In situ fibre fracture measurement in carbon–epoxy laminates using high resolution computed tomography, Composites Science and Technology 71 (12) (2011) 1471–1477. doi:10.1016/j.compscitech.2011.06.004.

[5] A. E. Scott, I. Sinclair, S. M. Spearing, A. Thionnet, A. R. Bunsell, Damage accumulation in a carbon/epoxy composite: Comparison between a multiscale model and computed tomography experimental results, Composites Part A: Applied Science and Manufacturing 43 (9) (2012) 1514–1522. doi:http://dx.doi.org/10.1016/j.compositesa.2012.03.011.

[6] A. Thionnet, H. Y. Chou, A. Bunsell, Fibre break processes in unidirectional composites, Composites Part A: Applied Science and Manufacturing 65 (0) (2014) 148–160. doi:http://dx.doi.org/10.1016/j.compositesa.2014.06.009.

[7] Y. Swolfs, L. Gorbatikh, I. Verpoest, Fibre hybridisation in polymer composites: A review, Composites Part A: Applied Science and Manufacturing 67 (0) (2014) 181–200. doi:http://dx.doi.org/10.1016/j.compositesa.2014.08.027.

[8] S. Pimenta, Fibre failure modelling, in: P. P. Camanho, S. R. Hallet (Eds.), Numerical Modelling of Failure in Advanced Composite Materials, Woodhead Publishing, 2015, Ch. 25.

[9] S. L. PHOENIX, I. J. BEYERLEIN, Statistical Strength Theory for Fibrous Composite Materials, Comprehensive Composite Materials (2000) 559–639doi:10.1016/B0-08-042993-9/00056-5.

[10] J. M. Hedgepeth, Stress Concentrations in Filamentary Structures, Tech. rep., NASA Langley Research Center; Hampton, VA United States (1961).

[11] Y. Swolfs, L. Gorbatikh, V. Romanov, S. Orlova, S. V. Lomov, I. Verpoest, Stress concentrations in an impregnated fibre bundle with random fibre

packing, Composites Science and Technology 74 (0) (2013) 113–120. doi:http://dx.doi.org/10.1016/j.compscitech.2012.10.013.

[12] H. E. Daniels, The Statistical Theory of the Strength of Bundles of Threads. I, Proceedings of the Royal Society of London A: Mathematical, Physical and Engineering Sciences 183 (995) (1945) 405–435. doi:10.1098/rspa.1945.0011.

[13] B. W. Rosen, Tensile failure of fibrous composites, AIAA Journal 2 (11) (1964) 1985–1991. doi:10.2514/3.2699.

[14] W. A. Curtin, Theory of Mechanical Properties of Ceramic-Matrix Composites, Journal of the American Ceramic Society 74 (11) (1991) 2837–2845. doi:10.1111/j.1151-2916.1991.tb06852.x.

[15] D. G. Harlow, S. L. Phoenix, The chain-of-bundles probability model for the strength of fibrous materials I: analysis and conjectures, Journal of composite materials 12 (2) (1978) 195–214.

[16] I. J. Beyerlein, S. Phoenix, Stress concentrations around multiple fiber breaks in an elastic matrix with local yielding or debonding using quadratic influence superposition, Journal of the Mechanics and Physics of Solids 44 (12) (1996) 1997–2039. doi:http://dx.doi.org/10.1016/S0022-5096(96)00068-3.

[17] T. Okabe, N. Takeda, Y. Kamoshida, M. Shimizu, W. A. Curtin, A 3D shear-lag model considering micro-damage and statistical strength prediction of unidirectional fiber-reinforced composites, Composites Science and Technology 61 (12) (2001) 1773–1787. doi:http://dx.doi.org/10.1016/S0266-3538(01)00079-3.

[18] T. Okabe, H. Sekine, K. Ishii, M. Nishikawa, N. Takeda, Numerical method for failure simulation of unidirectional fiber-reinforced composites with spring element model, Composites Science and Technology 65 (6) (2005)

921–933. doi:http://dx.doi.org/10.1016/j.compscitech.2004.10.030.

[19] Y. Swolfs, H. Morton, A. Scott, L. Gorbatikh, P. Reed, I. Sinclair, S. Spearing, I. Verpoest, Synchrotron radiation computed tomography for experimental validation of a tensile strength model for unidirectional fibre-reinforced composites, Composites Part A: Applied Science and Manufacturing 77 (2015) 106–113. doi:10.1016/j.compositesa.2015.06.018.

[20] R. P. Tavares, A. R. Melro, M. A. Bessa, A. Turon, W. K. Liu, P. P. Camanho, Mechanics of hybrid polymer composites : analytical and computational study, Computational Mechanics 57 (3) (2016) 405–421. doi:10.1007/s00466-015-1252-0.

[21] R. P. Tavares, F. Otero, A. Turon, P. P. Camanho, Effective simulation of the mechanics of longitudinal tensile failure of unidirectional polymer composites, International Journal of Fracture 208 (1-2) (2017) 269–285. doi:10.1007/s10704-017-0252-9.

[22] J. Guerrero, J. Mayugo, J. Costa, A. Turon, A 3D Progressive Failure Model for predicting pseudo-ductility in hybrid unidirectional composite materials under fibre tensile loading, Composites Part A: Applied Science and Manufacturing 107 (2018) 579–591. doi:10.1016/J.COMPOSITESA.2018.02.005.

[23] L. St-Pierre, N. J. Martorell, S. T. Pinho, Stress redistribution around clusters of broken fibres in a composite, Composite Structuresdoi:10.1016/j.compstruct.2017.01.084.

[24] S. Pimenta, S. T. Pinho, Hierarchical scaling law for the strength of composite fibre bundles, Journal of the Mechanics and Physics of Solids 61 (6) (2013) 1337–1356. doi:http://dx.doi.org/10.1016/j.jmps.2013.02.004.

[25] J. M. Hedgepeth, P. Van Dyke, Local Stress Concentrations in Imperfect Filamentary Composite Materials, Journal of Composite Materials 1 (3) (1967) 294–309. doi:10.1177/002199836700100305.

[26] A. Bunsell, L. Gorbatikh, H. Morton, S. Pimenta, I. Sinclair, M. Spearing, Y. Swolfs, A. Thionnet, Benchmarking of strength models for unidirectional composites under longitudinal tension, Composites Part A: Applied Science and Manufacturingdoi:10.1016/J.COMPOSITESA.2018.03.016.

[27] Y. Swolfs, I. Verpoest, L. Gorbatikh, Issues in strength models for unidirectional fibre-reinforced composites related to Weibull distributions, fibre packings and boundary effects, Composites Science and Technology 114 (2015) 42–49. doi:10.1016/j.compscitech.2015.04.002.

[28] A. R. Melro, P. P. Camanho, S. T. Pinho, Generation of random distribution of fibres in long-fibre reinforced composites, Composites Science and Technology 68 (9) (2008) 2092–2102. doi:http://dx.doi.org/10.1016/j.compscitech.2008.03.013.

[29] T. Okabe, K. Ishii, M. Nishikawa, N. Takeda, Prediction of Tensile Strength of Unidirectional CFRP Composites, Advanced Composite Materials 19 (3) (2010) 229–241. doi:10.1163/092430409X12605406698273.

[30] B. Delaunay, Sur la sphere vide, Izv. Akad. Nauk SSSR, Otdelenie Matematicheskii i Estestvennyka Nauk 7 (793-800) (1934) 1–2.

[31] W. Weibull, A Statistical Distribution Function of Wide Applicability, Journal of Applied Mechanics - Transactions of the ASME. 58 (7) (1951) 1001–1010.

[32] M. Nishikawa, T. Okabe, N. Takeda, Determination of interface properties from experiments on the fragmentation process in single-fiber composites, Materials Science and Engineering A 480 (1-2) (2008) 549–557. doi:10.1016/j.msea.2007.07.067.

[33] M. J. DeJong, M. A. Hendriks, J. G. Rots, Sequentially linear analysis of fracture under non-proportional loading, Engineering Fracture Mechanics 75 (18) (2008) 5042–5056. doi:10.1016/j.engfracmech.2008.07.003.

[34] J. G. Rots, S. Invernizzi, Regularized sequentially linear saw-tooth softening model, International Journal for Numerical and Analytical Methods in Geomechanics 28 (78) (2004) 821–856. doi:10.1002/nag.371.

[35] H. L. Cox, The elasticity and strength of paper and other fibrous materials, British Journal of Applied Physics 3 (3) (1952) 72–79. doi:10.1088/0508-3443/3/3/302.

[36] C. M. Landis, R. M. McMeeking, A shear-lag model for a broken fiber embedded in a composite with a ductile matrix, Composites Science and Technology 59 (3) (1999) 447–457. doi:10.1016/S0266-3538(98)00091-8.

[37] X. F. Zhou, H. D. Wagner, Stress concentrations caused by fiber failure in two-dimensional composites, Composites Science and Technology 59 (7) (1999) 1063–1071. doi:10.1016/S0266-3538(98)00145-6.

[38] I. J. Beyerlein, S. Phoenix, Statistics for the strength and size effects of microcomposites with four carbon fibers in epoxy resin, Composites Science and Technology 56 (1) (1996) 75–92. doi:http://dx.doi.org/10.1016/0266-3538(95)00131-X.

[39] W. A. Curtin, N. Takeda, Tensile Strength of Fiber-Reinforced Composites: II. Application to Polymer Matrix Composites, Journal of Composite Materials 32 (22) (1998) 2060–2081. doi:10.1177/002199839803202204.

[40] W. A. Curtin, Dimensionality and size effects on the strength of fiber-reinforced composites, Composites Science and Technology 60 (4) (2000) 543–551. doi:http://dx.doi.org/10.1016/S0266-3538(99)00150-5.

[41] Y. Swolfs, R. M. McMeeking, I. Verpoest, L. Gorbatikh, The effect of fibre dispersion on initial failure strain and cluster development in unidirectional

carbon/glass hybrid composites, Composites Part A: Applied Science and Manufacturing 69 (0) (2015) 279–287. doi:http://dx.doi.org/10.1016/j.compositesa.2014.12.001.